

Highly Flexible Single-Unit Resolution All Printed Neural Interface on a Bioresorbable Backbone

Reem M. Almasri, Walid AlChamaa, Ali Reza Tehrani-Bagha, and Massoud L. Khraiche*



Cite This: *ACS Appl. Bio Mater.* 2020, 3, 7040–7051



Read Online

ACCESS |



Metrics & More



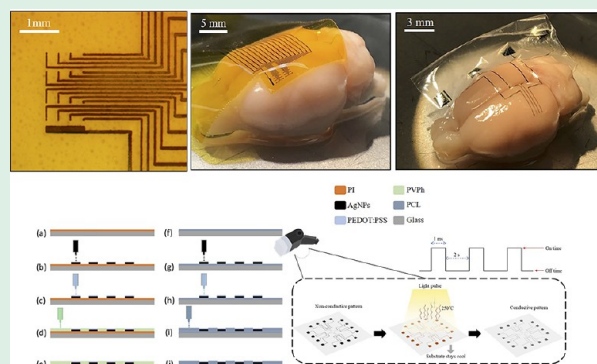
Article Recommendations



Supporting Information

ABSTRACT: Neural interfaces are the parts of the neural prosthesis that are in contact with the target tissue. The mechanical, chemical, and electrical properties of these interfaces can be a major determinant of the life of the implant and the neural tissue for chronic and even acute integrations. In this work, we developed a fully inkjet-printed, flexible neural interface on a bioresorbable backbone capable of recording high-fidelity neural activity. We utilized room temperature fabrication processes that overcome the limitations of semiconductor fabrication techniques for processing low-melting point polymers while maintaining high spatial and single-cell recording resolution. The $\sim 8 \mu\text{m}$ -thick devices in this study were fabricated onto two flexible polymers: (a) polyimide (PI), a biocompatible polymer commonly used for neural interfaces, and (b) polycaprolactone (PCL), a bioresorbable polyester with outstanding mechanical properties. Electrodes for neural recording were built at 30, 50, 75, and 100 μm diameter using silver nanoparticles/(3,4-ethylenedioxythiophene)–poly(styrenesulfonate) (AgNPs/PEDOT:PSS), which through our process achieved the lowest impedance reported in the literature reaching $\sim 200 \Omega$ at 1 kHz for a 50 μm electrode diameter. We further enhanced the electrochemical performance of AgNPs/PEDOT:PSS by an order of magnitude by incorporating exfoliated graphene into the electrodes. The biocompatibility of the fabricated devices and their ability to record single-unit activity were confirmed by *in vitro* tests on both rat PC12 cells and isolated neural rat retina, respectively.

KEYWORDS: neural interface, electrodes, single unit, biodegradable, flexible, PEDOT:PSS



INTRODUCTION

Neural interfaces play a major role in prosthetic intervention aimed at the treatment and management of neurological diseases.^{1–3} These interfaces consist of the component of a neural prosthesis that is in intimate contact with target tissue and where signal transduction occurs for neural recording or modulation. That being said, the complexity of acute or chronic integration of an electronic device with neural tissue (especially at the interface) has limited the life and efficiency of clinical prosthetic intervention. This is due to several challenges including: tissue and implant damage caused by unwanted chemical reactions at the electrodes, damage due to invasive surgeries for device resection in the case of patients requiring postoperative monitoring,² and mechanical mismatch between the neural tissue and the implant inducing stress on the tissue. These challenges also lead to a foreign body response that isolates the device from the targeted neural tissue and reduces its functional lifespan.^{3,4} To address this, much of the innovation in neural interfaces has been focused on new materials, specifically for implant backbone and electrode materials with high electrochemical performance. The choice of materials is limited by process compatibility with semiconductor fabrication, which is commonly used to build

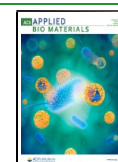
functional neural interfaces to achieve high spatial and single-cell resolution. A very basic neural interface has to go through high temperatures and withstand harsh chemicals. This precludes the use of highly flexible polymer backbones that are thermally and chemically incompatible. An example of polymers used as a backbone for neural interfaces is polyimide (PI), which is known for its superior thermal and chemical resistance, excellent electrical and thermal insulation of metallic conductors, biocompatibility, and high elasticity.^{5,6} On the other hand, PI suffers from mechanical mismatch with brain tissue due to its high Young's modulus (PI = 2.7 GPa, brain tissue = 2 KPa).^{5,7}

Inkjet printing has emerged as an attractive drop-on-demand patterning technique that directly jets various types of functional materials with micron resolution.⁸ Advances in material dispensing technologies and accurate electronic

Received: July 19, 2020

Accepted: September 14, 2020

Published: September 14, 2020



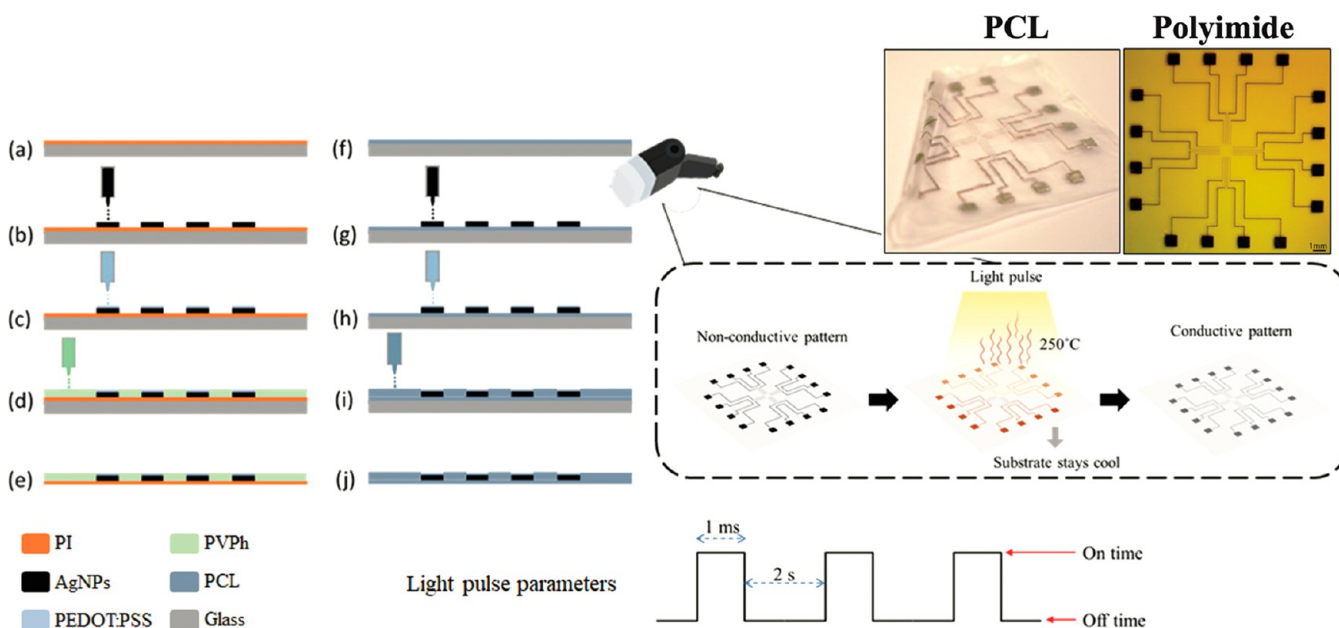


Figure 1. Schematic illustration of the fabrication and sintering process of AgNPs/PEDOT:PSS electrodes. (a) PI substrate. (b) Ag ink is patterned to form leads and cured. (c) PEDOT:PSS is printed to form electrodes. (d) PVPh is printed to insulate. (e) PI device is released from the glass substrate. Process for PCL. (f) Spin coating PCL. (g) Ag ink is patterned to form leads and flash sintered. (h) PEDOT:PSS printed to form electrodes. (i) PCL is printed to insulate. (j) PCL device released from glass.

alignment has increased speed and resolution of inkjet printing to a large extent. This method creates contactless and maskless patterns by sequentially depositing multiple layers of different materials without perturbing the previously deposited layers. The additive nature of this process makes it suitable to deposit a variety of conductive and insulation materials including solvent-based and aqueous-based materials, particle suspensions, UV-curable fluids, and biological solutions on a variety of substrates, such as organic and inorganic substrates and flexible and stiff substrates, in addition to the conventional silicon wafers. Recently, inkjet printing has attracted interest in building electrodes for neural interfaces.^{9–12} However, none of these devices achieved the performance metrics needed to reach single-cell resolution. Also, these efforts were only partially inkjet printed and relied on coating methods to insulate leads that reduced spatial resolution. In addition, these devices were fabricated on substrates that suffer from mechanical mismatch with neural tissue.

In this work, we developed an inkjet-printed, biodegradable, and highly flexible neural interface that exhibits high electrochemical performance and is capable of recording single-unit activity. The room temperature inkjet process coupled with photonic sintering enabled the fabrication of silver nanoparticles (AgNPs)/(3,4-ethylenedioxythiophene)–poly(styrenesulfonate) electrodes onto a low-melting temperature, highly conformable, and biodegradable polymer (polycaprolactone (PCL)).

For electrode material, we utilized (3,4-ethylenedioxythiophene)–poly(styrenesulfonate) (PEDOT:PSS), a polystyrenesulfonate polymer mixture of two ionomers, sodium polystyrenesulfonate and poly(3,4-ethylenedioxythiophene). This organic semiconductor contains sulfonyl groups that are deprotonated and carry a negative charge, and PEDOT is a conjugated polymer that carries a positive charge. PEDOT:PSS is known for its biocompatibility,¹³ long-term stability,¹⁴ solution processability, electrical conductivity,¹⁵ and signal-

to-noise ratio (SNR) enhancement for recording and stimulating electrodes.¹⁶ We compared the electrical and mechanical properties of the neural electrodes built on PCL to electrodes built on PI (typical substrate material for neural interfaces). We also optimized the electrochemical performance by investigating the impact of the number of PEDOT:PSS coating layers and electrode diameter. In addition, we further enhanced the electrochemical properties of the PEDOT:PSS electrodes by introducing graphene/PEDOT:PSS ink; its performance was comparable to 7 layers of PEDOT:PSS. The device was tested with neural tissue *in vitro* using an excised retinal preparation.

■ MATERIALS AND METHODS

Materials. PCL pellets ($M_w \sim 48\,000$ – $90\,000$ Da), PEDOT:PSS aqueous solution (solid content 1.3 wt %), graphene/PEDOT:PSS hybrid ink (electrochemically exfoliated), silver nanoparticle (AgNP) ink, poly(4-vinylphenol) (PVPh), poly(melamine-co-formaldehyde), and PLGA (75:25) were purchased from Sigma-Aldrich, USA. All chemicals used in the electrophysiology and biocompatibility experiments as well as the electrochemical characterization, including phosphate buffer saline (PBS), sodium bicarbonate, Ames' medium, Trypan Blue (TB), and Dulbecco's Modified Eagle's Medium (DMEM), supplemented with 10% fetal bovine serum and 1% Pen/Strep (antibiotics), were also purchased from Sigma-Aldrich, USA. All solvents, including chloroform, dimethylformamide (DMF), dimethyl sulfoxide (DMSO), and 1-hexanol were of the highest purity commercially available from Sigma-Aldrich and were used without further purification. PI films of 7 μm thickness were purchased from DuPont, USA. Deionized water was utilized in the entire experiment.

Substrate and Ink Preparation. PI substrates were extensively rinsed using 70% ethanol and dried with a nitrogen gun prior to the printing process. PCL substrates were prepared with 20% w/v PCL of 9:1 chloroform to DMF. The pellets were added to chloroform and stirred at 50 °C for 30 min. DMF was then added and mixed after visually ensuring that all the pellets were completely dissolved. A spin coater (WS-650MZ-23NPPB, Laurell Technologies Corporation) was used to prepare the 7 μm PCL films with 1000 rpm and 5 min of spinning duration.

The conductive patterns were inkjet printed using a commercially available AgNP ink at a concentration of 50–60 wt % in tetradecane (average diameter of NP is 10 nm). Two conductive coatings were used, PEDOT:PSS and graphene/PEDOT:PSS. In detail, PEDOT:PSS solution was diluted with DI water. DMSO and Triton X-100 were added at 5% and 1% concentrations, respectively, to enhance the conductivity of the solution.^{17,18} The resulting dilution of 1:1 PEDOT:PSS/H₂O + 5% DMSO + 1% Triton X-100 brought PEDOT:PSS to the preferable ink properties. Graphene/PEDOT:PSS ink consisted of PEDOT:PSS at a concentration of 0.2 mg/mL and graphene with a concentration of 1 mg/mL, all dispersed in DMF. For the passivation of electrode leads, two formulations were prepared to match the substrate material. For the PI-based interface, a polymer-based ink was formulated using 1-hexanol as a solvent material (ratio of 17:1 w/w% of 1-hexanol to the polymers). The polymer recipe is composed of PVPPh and PMF with a 1:1 w/w% ratio. For the PCL-based interface, a PCL ink was formulated using chloroform as a solvent with a 3% w/v ratio.

Fabrication of Inkjet-Printed Ag Electrode. The printing process was done via a commercially available material printer (DMP-2850, Fujifilm Dimatix, USA) fitted with a piezo-driven 16-nozzle print head. The conductive patterns and coatings were printed using a 1 pL cartridge, while the passivation layers were printed using a 10 pL cartridge. The fabrication process of the PI-based and PCL-based arrays is illustrated in Figure 1. The PCL- and PI-based electrodes were printed with the AgNP ink at room temperature. This ink requires a sintering process at high temperatures up to 250 °C to trigger the nanoparticles to coalesce. The PI-based pattern was thermally sintered at 250 °C on a hot plate. However, due to the heat-sensitive nature of the chosen PCL substrate, a room temperature photonic sintering technique was employed. This approach uses intense light pulses for a few milliseconds to instantly increase the temperature of the printed pattern up to 250 °C while leaving the majority of the substrate relatively cool. To achieve that, a camera flash lamp (Nikon Speedlight SB-28) with two consecutive pulses of 1 ms pulse width and off period of 2 s was used. The PCL substrate was placed 1 cm away from the light source, and an aluminum reflector was placed around the substrate to uniformly distribute the light on the overall pattern. The diameter of the electrodes was varied between 30 and 100 μm, and the electrodes were coated with up to 10 layers of PEDOT:PSS on top of each other. The printed coating films on the PI-based electrodes were annealed at 90 °C for 3 h in order to remove all residual liquid. The coating films on PCL-based electrodes were left overnight to dry completely. The PVPPh dielectric ink was deposited on the PI-based array and cured at 200 °C for 1 h on a hot plate to allow cross-linking. The PCL dielectric ink was deposited on the PCL-based array and left to dry at room temperature without any further curing.

Characterization of the Interface. The elemental composition of the AgNPs was characterized by scanning electron microscopy (SEM; MIRA 3 LMU Tescan, Czech Republic). The wettability of the substrates was measured by a standard optical tensiometer (OCA 15EC, Dataphysics, Germany) with the sessile drop method analysis. The thickness and roughness of the printed conductive coatings were measured using a Bruker DEKTAK-Xt profilometer. A four-point probe system (Ossila, UK) was used to measure the resistance of the printed patterns. The mechanical properties of the prepared interfaces were determined, including the elastic moduli, using a mechanical testing machine (Instron, Norwood, MA) with a 10 N load cell at a strain rate of 50 mm/min. To measure the viscosity and surface tension of the inks, a rotational viscometer (FungiLab SA, Spain) and goniometer OCA 15EC were used, respectively.

The electrochemical performance of the PEDOT:PSS- and graphene/PEDOT:PSS-coated electrodes as a function of the number of layers and surface area was measured by a Potentiostat/Galvanostat/ZRA system (Gamry Instruments, USA) using a three-electrode cell. A glass beaker was filled with PBS, and platinum (Pt) was used as a counter electrode while Ag/AgCl was used as a reference electrode. Electrochemical impedance spectroscopy (EIS) and cyclic voltammetry (CV) techniques were mainly adapted to

assess the impedance and Charge Injection Capacity (CSC) of the electrodes. As for the CV, the voltage was swept between −0.5 and 0.5 V at a rate of 100 mV/s. The same system was used to evaluate and compare the performance of the PCL-based electrodes to PI-based ones. The circuit model fitting was done on a Gamry Echem Analyst (Version 6.33).

Electrophysiology. Electrophysiological recording experiments were conducted in order to investigate the feasibility of inkjet-printed flexible electrodes as a reliable neural interface. Retinas were dissected from carbon dioxide euthanized eyes that were obtained from Sprague/Dawley rats.^{19,20} Sodium bicarbonate was used to buffer the Ames' medium, and then, it was oxygenated to bring the medium pH to 7.4. Retinas were dissected into 4 × 4 mm retinal segments and were kept in the Ames' solution at 37 °C. The retina segment was transferred onto the prepared device, which was connected to the ME2100 system (Multi-Channel Systems, Germany). A chamber over the active area of the device was attached to add media to the cells. The extracted retina was placed with the ganglion cells (GC) facing the electrodes. To enhance tissue adhesion and increase the wettability of the surface, the arrays were ozone cleaned in the UV + ozone chamber for 45 min before placing the retina. The system was equipped with a perfusion system to supply the tissue with a fresh solution and maintain viability for the longest time. Offline sorter software (Plexon Inc., Dallas, TX) was used to analyze the data and detect the spiking activity. A threshold was set as 4 times standard deviation of the background noise to detect the single spike units.²¹ The recorded spikes passing the threshold were then fitted to preloaded templates matching features of neuronal spike activity. Recordings were collected simultaneously from all designed electrodes.²²

For light response experiments, a 500 ms squared pulse with an intensity of 5 V was generated via a programmed Arduino microcontroller to trigger the LED circuit, which involves a white LED connected in series to a 61.9 Ω resistor. This corresponds to a high photopic light stimulus comparable to broad daylight that effectively activates cone photoreceptors. Single pulses every 2 s were utilized to optically stimulate the retina.

Biocompatibility and Degradability. PC12 cells were used to verify biocompatibility on the PI- and PCL-based arrays. The cells were cultured in DMEM and maintained in a humidified incubator at 37 °C with 5% CO₂. At 80% cell confluency, the cells were dissociated with trypsin, centrifuged, and resuspended in fresh medium for seeding. The entire cell culture process was performed in laminar flow hood (LabGard, Class II, Type A2 Biosafety Cabinet, USA) to prevent contamination.

For cell culture experiments, PI-based arrays were sterilized by autoclaving with a ramping temperature up to 132 °C for 30 min. On the other hand, PCL-based arrays were fixed on a Petri dish with silicone as an adhesive, sterilized by UV light irradiation (type C) with an intensity of 100 μW/cm² for 6 h, and then equilibrated in sterile 1× PBS for 24 h. Each array was immersed in medium inside a separate Petri-dish for a few minutes before cell seeding. PC12 cells were distributed on the substrates by dripping using a glass pipet. The adhesion behavior and morphology of the cells were monitored every 24 h using a phase-contrast inverted microscope. Tissue culture plastic (TCP) was used as a positive control.

The viability of the cells was assessed by the TB exclusion assay. Generally, the dye in TB penetrates the compromised cell membranes of dead cells, staining them with dark blue color. The percentage of living cells was determined by counting the live and dead cells using ImageJ software. The results from the printed PI and PCL substrates were compared to the ones without arrays (i.e., control sample). This control will ensure nothing in the processing could cause cytotoxicity. In addition, the results taken from the PI and PCL substrates were compared to the TCP control values.

The designed interface in this study is made to degrade after the whole brain monitoring process, which is clinically predefined, is done or when the electrodes stop functioning completely. On the basis of PCL properties mentioned in the literature,²³ a complete degradation of PCL can take months to years, depending on its molecular weight.

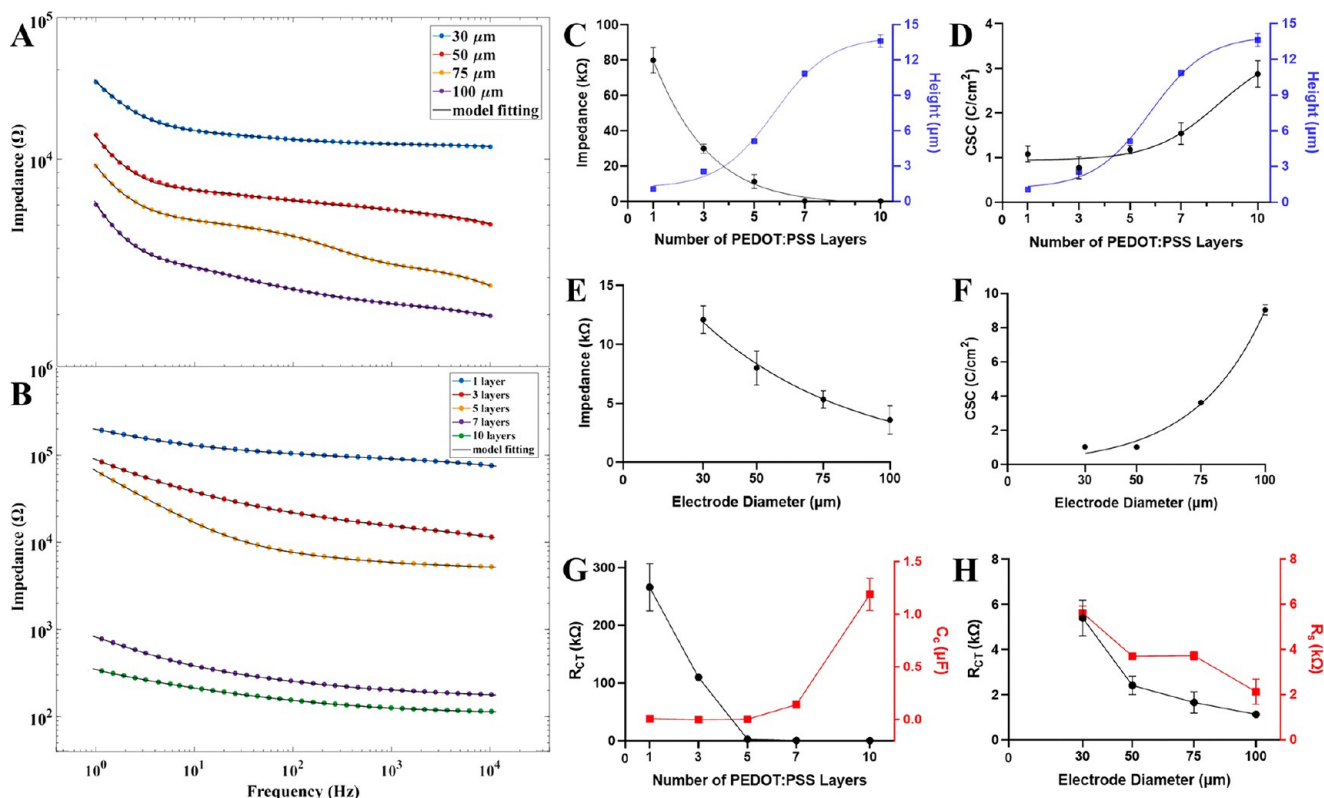


Figure 2. (A) EIS shows the impact of the PEDOT:PSS electrode diameter on electrode impedance. (B) EIS shows the impact of PEDOT:PSS multiple layer printing on 50 μm electrode impedance (lower impedance results in lower recording noise). (C, D) Shows the change in impedance at 1 kHz (decrease) and the CSC (increase) with an increase in the number of PEDOT:PSS layers. (E, F) Shows the change in impedance at 1 kHz (decrease) and the CSC (increase) with an increase in the electrode area. (G) Resistance RCT and capacitance CC at 1 kHz as a function of the number of PEDOT:PSS layers. (H) Resistance RCT and RS at 1 kHz as a function of electrode diameter. Error bars are the result of measuring 8 printed electrodes from 6 different devices for each data point.

Table 1. Comparison of the Electrochemical Performance of Some of the Best Performing Coating Methods Used to Fabricate PEDOT:PSS Neural Electrodes^a

coating material	deposition method	thickness [μm]	impedance at 1 kHz [$\text{k}\Omega$]	charge storage capacity [C cm^{-2}]	ref
PEDOT:PSS	inkjet printing	13.6	0.2	2.876	this work
PEDOT:PSS	spin-casting		15		25
PEDOT:PSS	spin-casting	0.103	50	0.582	26
PEDOT:PSS/GOPS	spin-casting	0.35	8		27
PEDOT:PSS/GOPS	electrodeposition	0.35	8		27
PEDOT:PSS/PEG	electrodeposition		5.4		28

^a50 μm diameter.

Nonetheless, the surface area of the implant also plays a role in the degradation rate. Lifetime assessment to an implant with such high reliability is an important issue to determine its actual functional lifespan. Due to the high cost of the biodegradation test *in vivo*, an accelerated chemical hydrolysis in NaOH was employed instead.²⁴ This accelerated degradation test helps in assessing the lifetime of the PCL backbone. The arrays ($22 \times 22 \times 0.008$ mm) were entirely immersed in the prepared aqueous buffer solution (pH 13) at 37 °C. This system involves ~ 1 μm , ~ 1.1 μm , ~ 95 nm, and ~ 7 μm thick layers of the PCL passivation layer, PEDOT:PSS, Ag, and PCL substrate, respectively. To demonstrate the feasibility of tuning the degradation rate of the interface, a blend of PCL/PLGA (8:2) was also prepared to accelerate the degradation process. Under these conditions, the degradation behavior was monitored by taking a series of macroscopic images every 30 min while the temperature was held constant.

RESULTS AND DISCUSSION

Electrochemical Performance of Inkjet-Printed AgNPs/PEDOT:PSS Electrodes. The electrochemical performance of neural electrodes can give insight into their potential for recording small signals (single-cell activity) or the amount of charge they can deliver without damage for neuromodulation. We investigated the electrochemical performance of inkjet-printed PEDOT:PSS electrodes for both electrode diameter and electrode thickness. Figure 2A,B shows the impedance spectra of the microelectrodes for different electrode diameters and layers of PEDOT:PSS. At a constant diameter of 50 μm , the number of PEDOT:PSS coating layers was varied from 1 to 10. Figure 2C shows the progressive decrease of the mean impedance as the number of PEDOT:PSS layers increased. The impedance spectra follow a small resistive trend in frequencies less than 100 Hz, followed

by a capacitive trend in frequencies more than 100 Hz. The lowest impedance value was achieved with 10 layers of PEDOT:PSS coating, reaching $\sim 200 \Omega$ at 1 kHz, which is the lowest recorded in the literature for PEDOT:PSS for any fabrication method. CSC represents the maximum charge that can be injected into a neural tissue without causing damage to the electrodes. The CSC values, obtained by calculating the area under the CV curve, reached its maximum of 2.876 C/cm^2 with the 10 layer coated electrode. Figure 2D shows a progressive increase in the CSC values as the number of PEDOT:PSS layers increased. Our literature survey showed how our impedance numbers and CSC compare to other published work (Table 1).

Using inkjet printing, we achieved the lowest impedance at 1 kHz and the highest CSC values for PEDOT:PSS electrodes recorded in the literature. The enhanced electrochemical performance attributed to the additive nature of the inkjet printing process allows for a thickness increase in the conductive coating with each deposited layer; thus, the overall effective surface area increased. We achieved 10 layers without changing the diameter of the electrodes. Also, the addition of AgNPs as a lead and beneath PEDOT:PSS helps in reducing the impedance significantly. This combination is similar to structures used in the charge collection in solar cells, which also achieve an ohmic and low resistance interface.²⁹

In addition, an equivalent circuit model (Figure 3) was fitted to our experimental data (Figure 2A,B, fitting presented as

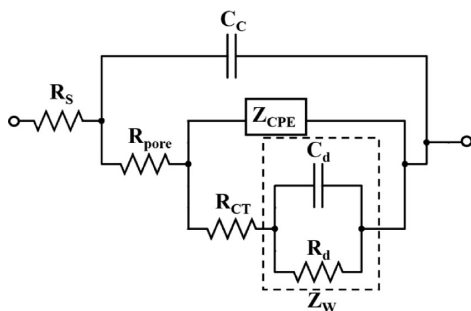


Figure 3. Equivalent circuit model of the electrode-coating-solution interface.

solid black lines). The Chi-Square goodness of fit test ($\chi^2 = 4.81 \times 10^{-4}$), for varying PEDOT:PSS layers, showed an

agreement between the experimental and fitted model. The coating capacitance (C_c) increased from 0.426 mF/cm^2 for 1 layer of PEDOT:PSS to 60.606 mF/cm^2 for 10 layers of PEDOT:PSS. This could be explained by the increase in the effective surface area because of the increase in the thickness of the PEDOT:PSS layer from 1.07 to $13.6 \mu\text{m}$. This is also in agreement with the increase in the CSC values from 1.083 to 2.876 C/cm^2 as shown in Figure 2D. This correlation between the coating capacitance (C_c) and the CSC values can be represented by the equation $C_c = ((\epsilon_0 \times \epsilon_r)/d)A$, where A is the electrode area, ϵ_0 is the dielectric permittivity of free space, ϵ_r is the relative dielectric permittivity of the medium between the two plates, and d is the distance between them. Moreover, the series resistance (R_s) and charge transfer resistance (R_{CT}) showed an inversely proportional relationship with the number of deposited layers (Figure 2G). The series resistance (R_s) dropped from $18.8 \text{ k}\Omega$ for 1 layer to $0.135 \text{ k}\Omega$ for 10 layers, while the charge transfer resistance (R_{CT}) dropped from $266 \text{ k}\Omega$ for 1 layer to $0.0471 \text{ k}\Omega$ for 10 layers. This shows the contribution of the increase in the effective surface area of the electrodes, given both resistances are proportional to $\rho/4r$, where ρ is the resistivity and r is the radius of the electrode.

Furthermore, the diameter of the electrode directly affects its electrochemical performance. As seen in Figure 2E,F, electrode diameter, ranging from 30 to $100 \mu\text{m}$, has a noticeable impact on the impedance magnitude as well as CSC values, respectively. Results from the model also confirm that both series resistance (R_s) and charge transfer resistance (R_{CT}) undergo a progressive decrease with respect to electrode diameter (Figure 2H). The series resistance (R_s) dropped from $5.61 \text{ k}\Omega$ for the $30 \mu\text{m}$ electrode to $2.13 \text{ k}\Omega$ for the $100 \mu\text{m}$ electrode, while the charge transfer resistance (R_{CT}) dropped from $5.39 \text{ k}\Omega$ for the $30 \mu\text{m}$ electrode to $1.13 \text{ k}\Omega$ for the $100 \mu\text{m}$ electrode. Similarly, the Chi-Square goodness of fit test ($\chi^2 = 1.14 \times 10^{-4}$) showed an agreement between the experimental and fitted model.

Graphene/PEDOT:PSS Electrodes. The electrochemical performance of PEDOT:PSS electrodes can be further enhanced by improving the conductivity of the organic semiconductor. The addition of exfoliated graphene to PEDOT:PSS showed a marked improvement in electrochemical performance versus PEDOT:PSS alone. Figure 4A,B shows the EIS and CV responses for $50 \mu\text{m}$ electrodes coated by a single layer of PEDOT:PSS versus a single layer of

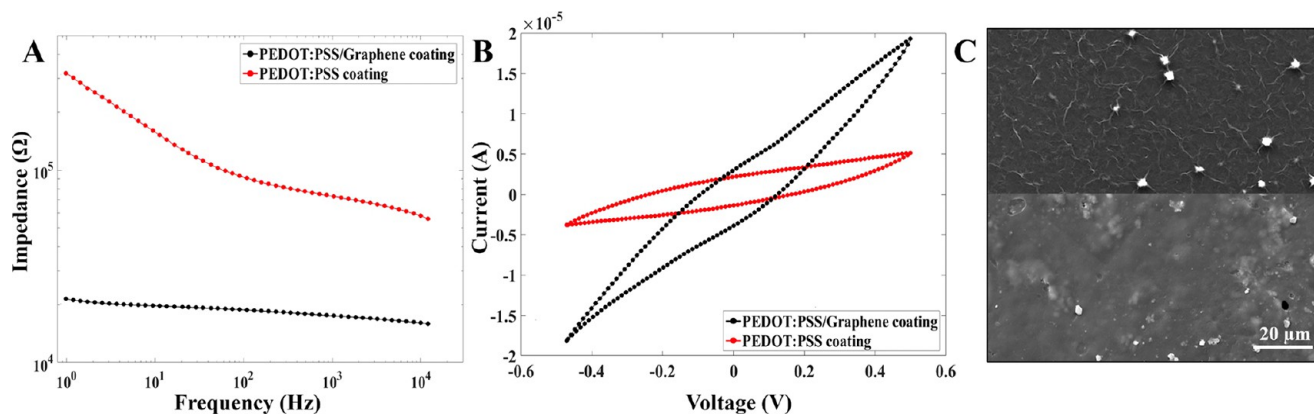


Figure 4. (A) EIS shows the impact of coating material on $50 \mu\text{m}$ electrode impedance (lower impedance with graphene/PEDOT:PSS coating). (B) CV plot shows the impact of coating material on $50 \mu\text{m}$ electrode CSC (higher CSC with graphene/PEDOT:PSS coating). (C) SEM images of the inkjet-printed graphene/PEDOT:PSS (upper) and PEDOT:PSS (lower) films showing the morphology of the surface.

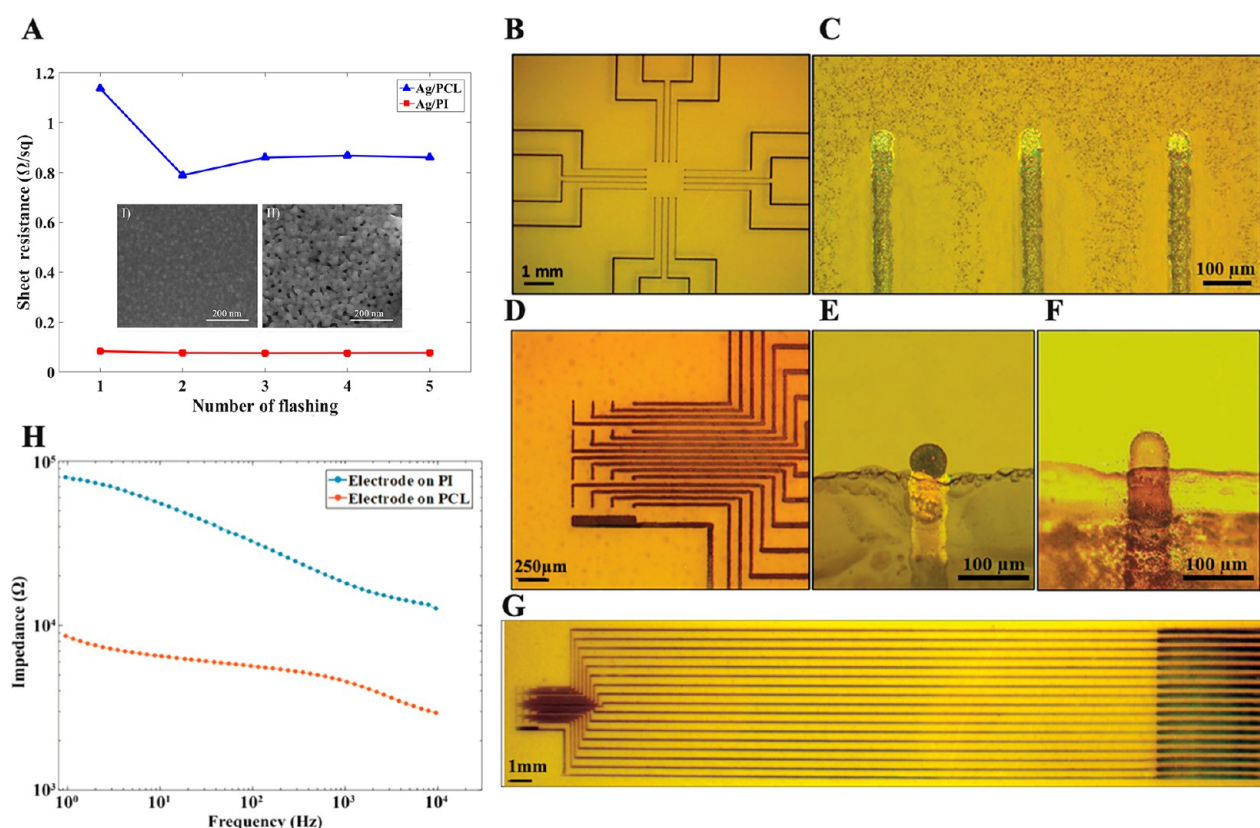


Figure 5. (A) The relationship between electrical resistance and the number of light pulses for sintering the inkjet-printed Ag patterns on the PI and PCL substrates. The inset SEM images of AgNPs: (I) before and (II) after sintering. (B) A 16-electrode neural interface printed on the PCL substrate. (C) Close-up of three individually insulated AgNPs/PEDOT:PSS electrode leads with a minimum wiring resolution of $30\ \mu\text{m}$ on the PCL substrate. (D) A 16-electrode neural interface printed on PI. The $50\ \mu\text{m}$ AgNP leads terminate with the PEDOT:PSS electrodes of $50\ \mu\text{m}$. (E, F) Close-up of $50\ \mu\text{m}$ AgNP leads terminate with graphene/PEDOT:PSS-coated (E) and PEDOT:PSS-coated (F) electrodes of $50\ \mu\text{m}$. The leads are passivated with PVPh. (G) A 16-electrode neural interface printed on PI with leads terminating at the zif board pads. (H) EIS shows the difference in impedance between electrodes printed on PI vs PCL.

graphene/PEDOT:PSS, respectively. The electrochemical performance for electrodes coated by graphene/PEDOT:PSS was enhanced compared to the one coated by PEDOT:PSS by more than an order of magnitude for the impedance. In fact, graphene/PEDOT:PSS coated electrodes showed low impedance and high CSC values that are nearly equivalent to 7 layers of PEDOT:PSS alone. This can be attributed to the fact that mixing conductive polymers like PEDOT:PSS with exfoliated graphene provides an additional electrochemical means to the electrodes. The degree of exfoliation and oxidation of the graphene solution plays a role in its electrical properties, as a higher degree of exfoliation leads to better dispersion of conductive graphene in the blend. Moreover, the unique arrangement of the carbon atoms in graphene facilitate a quick electron mobility without scattering, which saves the valuable energy that is typically lost in other conducting materials. The sheet resistance of pristine PEDOT:PSS is $52\ \text{k}\Omega/\text{sq}$, while in graphene/PEDOT:PSS, it is $0.5\ \text{k}\Omega/\text{sq}$.

In addition to improvement in the conductivity of graphene/PEDOT:PSS, the enhanced performance can be also due to the increase in the effective surface area (Figure 4C).^{30–32} Similar results are found for neural electrodes when CNT is incorporated into electrode materials.^{33,34} The measurements show that the mean surface roughness values for a single layer of PEDOT:PSS and graphene/PEDOT:PSS are ~ 59 and $\sim 135\ \text{nm}$, respectively.

Flash Sintering of Inkjet-Printed Electrodes. Ag ink was photonically sintered on both PI and PCL. Figure 5A demonstrates the sheet resistance of the inkjet-printed Ag with respect to flashing numbers. Both patterns that were printed on PI and PCL became conductive after the first light pulse. The lowest sheet resistance values obtained from photonically sintered patterns on PI and PCL substrates are $0.08 \pm 4.2 \times 10^{-4}$ and $0.789 \pm 4.2 \times 10^{-4}\ \Omega/\text{sq}$, respectively. SEM images of printed ink before and after sintering are shown in the inset figures in Figure 5A. The size of the NPs enlarges whenever thermal or light sintering is applied. In line with previous results of the sintering effect on the size of the NPs,³⁵ our findings showed that the diameter of the deposited AgNPs before sintering is $\leq 10\ \text{nm}$, while after sintering, the particles enlarged up to $\sim 50\ \text{nm}$, as an indication of the coalescence process. Patterns on the PI substrate have lower resistance values than those on PCL. When the light pulse is emitted, thermal radiation in the form of highly energized photons reaches the surface of the printed silver as well as the substrate in use. The AgNPs on the surface absorb a portion of the impinging radiation in order to coalesce, and the remaining energy is transmitted further down the thickness of the Ag ink via thermal conduction.³⁶ That way, AgNPs that are not exposed to the light pulse can still coalesce. However, since Ag has a high thermal diffusivity ($17200 \times 10^{-8}\ \text{m}^2/\text{s}$),³⁷ the conductive heat transmission is far more prevalent compared to the conversion of such heat to coalesce the NPs. This is

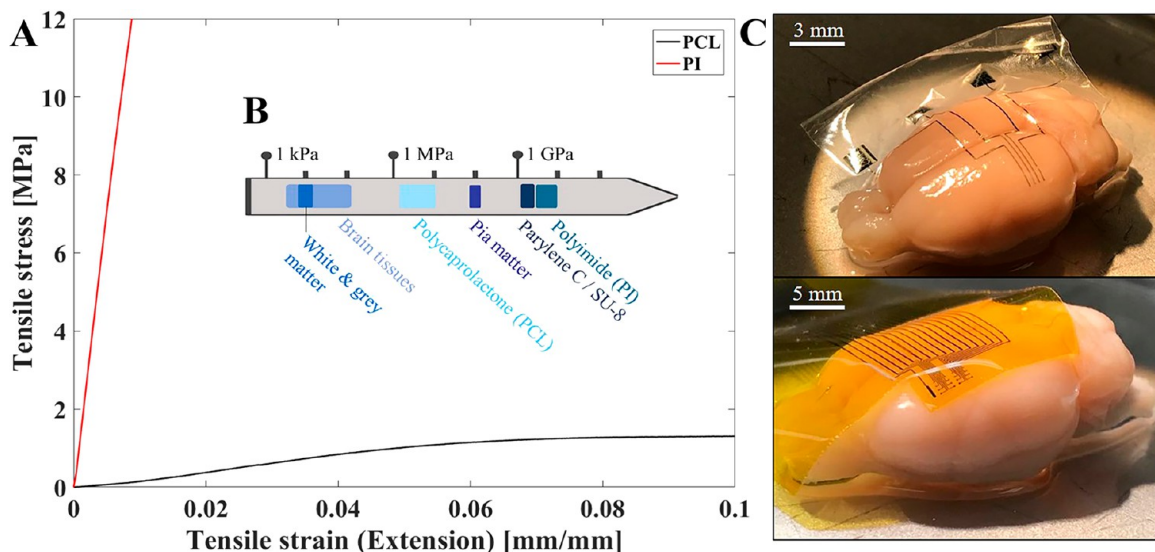


Figure 6. (A) Stress–strain analysis of PCL vs PI. (B) Schematic scaling that shows the mechanical properties of the brain tissue and the utilized polymers. (C) Microphotographic photos for soft conformal PCL-based (top) and PI-based (bottom) arrays showing electrodes lying on the surface of the rat brain.

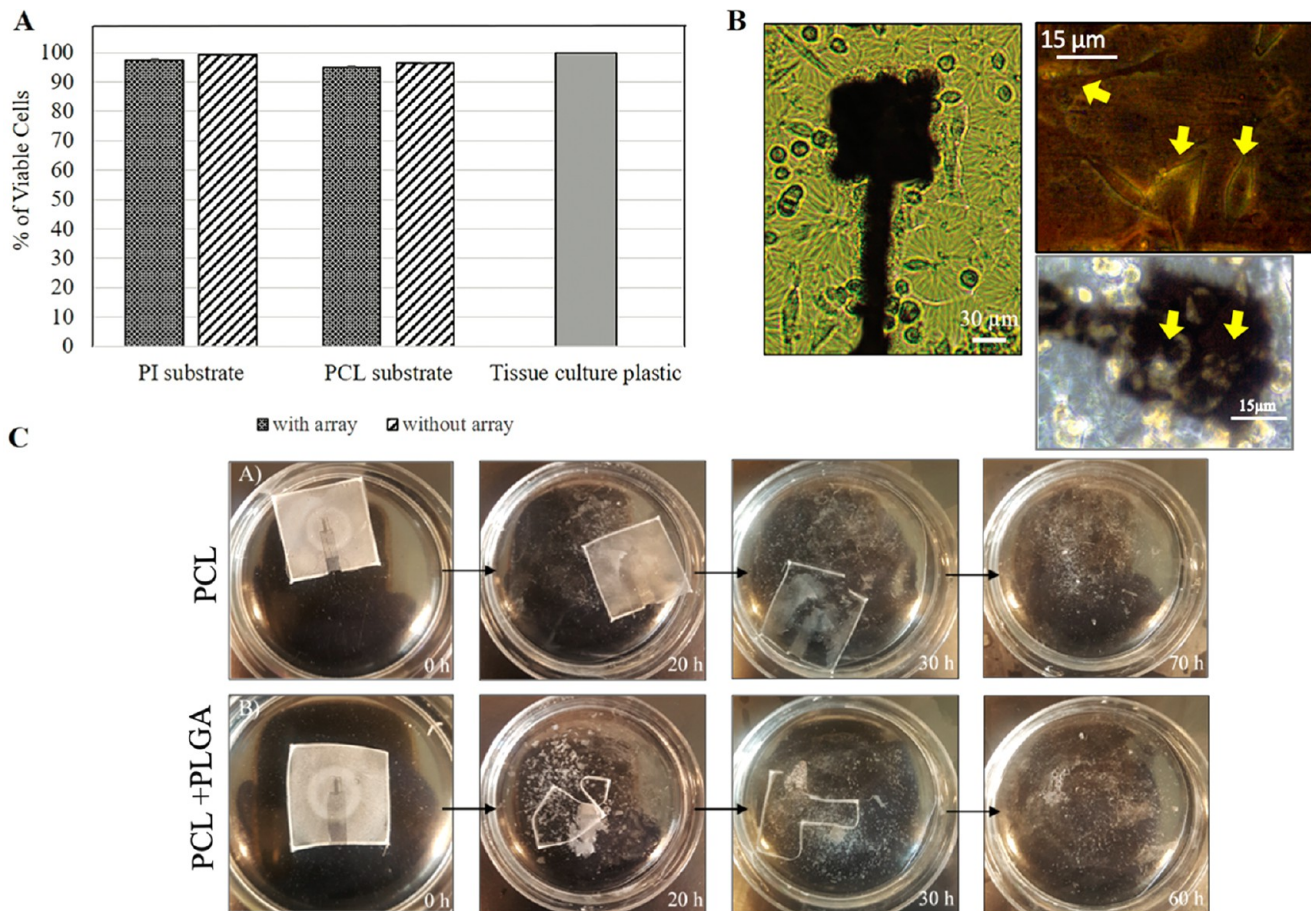


Figure 7. (A) The percentage of viable cells in the total cell population on the PI substrate, PCL substrate, and tissue culture plastic. Dark shaded bars represent biocompatibility on the substrate with arrays (PEDOT:PSS and AgNP lines). (B) PC12 cells on the PCL substrate surrounding and on top of the electrode. (C) Images collected at several stages of accelerated dissolution of (A) PCL and (B) PCL/PLGA interfaces immersed into an aqueous buffer solution (pH 13) at 37 °C.

especially true under such small time periods, and the implication is that a substantial amount of heat is readily transmitted to the silver–substrate interface.³⁸ The substrate’s

thermal diffusivity and its rate of heat absorption, in addition to the amount absorbed, need to be taken into consideration. This is because the substrate will inadvertently dissipate a

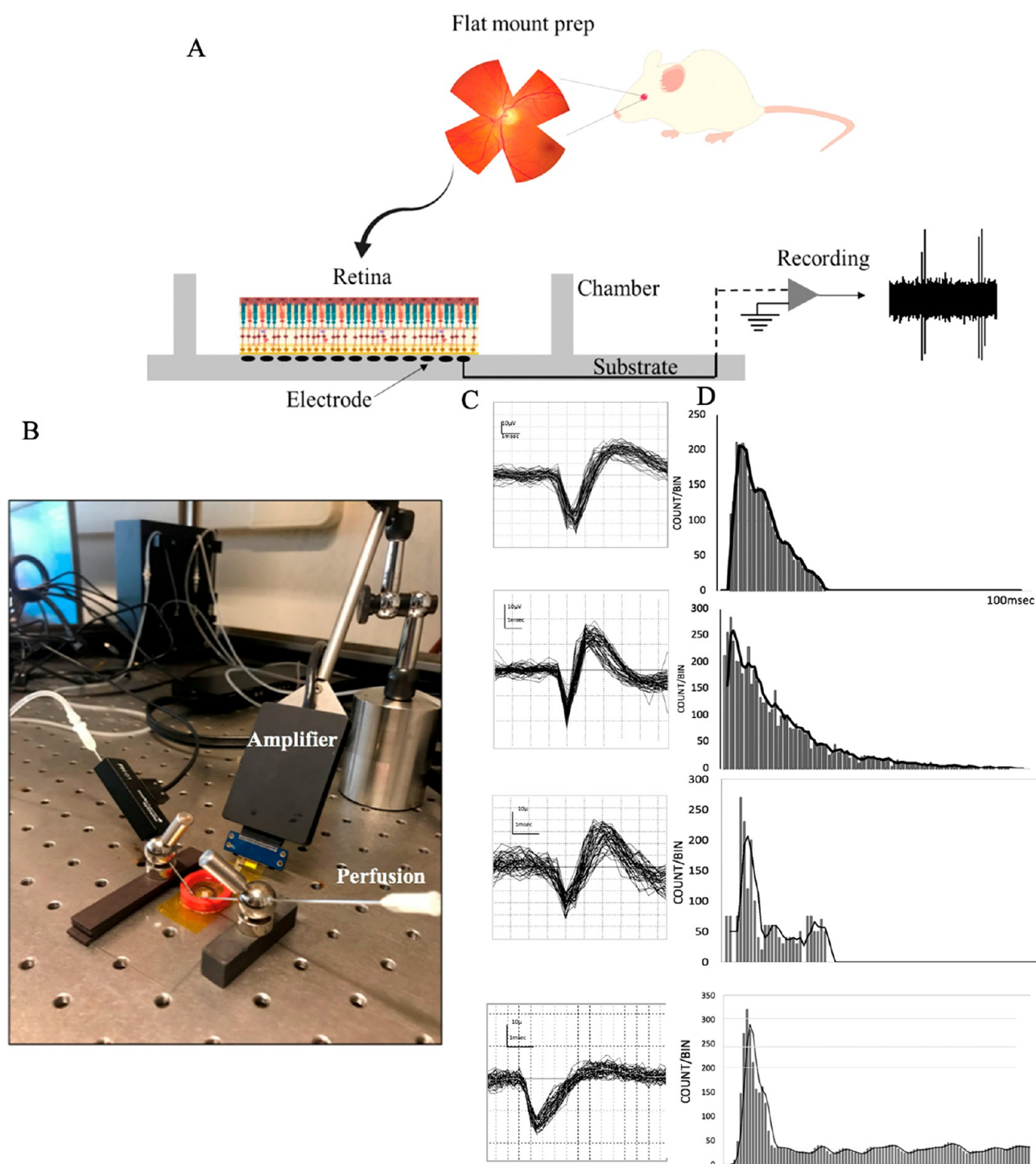


Figure 8. (A) Schematic of the general recording setup for measuring the electrophysiological activity from the retina. (B) Close-up of the recording setup where the printed array is connected to the ME2100 system via zif board. (C) Single-unit activity recorded by electrode arrays and detected by the spike sorter. (D) Interspike interval (ISI) of a rat retinal GC response to light stimuli.

noticeable amount of useful thermal energy that was meant to coalesce the NPs. For instance, the thermal diffusivity of PCL is 67.7% greater than that of PI.³⁹ This means that, under the same conditions, PCL will absorb a larger amount of any incoming heat (and at a higher rate) compared to PI. Therefore, low conductive pathways are formed because of this, which prevents the Ag from attaining the same sheet resistance value that could have been achieved if the NPs were thermally sintered. This problem also occurs in PI, but it is less

severe since the amount of heat absorbed is much lower in that small time period; so, the heat conduction is more prevalent in the horizontal direction. Images shown in Figure 5B–G show the various patterns and devices printed on both PCL and PI.

An electrochemical performance comparison between the electrodes on the PI and PCL substrates was conducted, on the basis of the fact that the post-treatment process of the printed PI- and PCL-based patterns differed, which consequently changed the adhesion, conductivity, and stability of the

electrodes. Figure 5H shows the impedance of electrodes on PI versus PCL, having the same surface area of $1963.5 \mu\text{m}^2$. The average impedance values for the electrodes printed on PI and PCL at 1 kHz are 4.57 and 18.08 k Ω , respectively (Figure 6A). As noticed, the electrodes on PI exhibit lower impedance and higher CSC. However, the electrochemical performance of the electrodes printed on PCL still fall within the acceptable range ($<5 \text{ M}\Omega$) for recording and stimulation from neural tissue.^{40–42}

Mechanical Characterization of the Interfaces. One of the key challenges facing implantable neural electrodes is the mechanical mismatch at the interface with neural tissue.^{43,44} This is a potential source of inflammation, immune response, scar formation, and physical damage of the surrounding tissue and the implant, which eventually diminish the signal resolution.^{45,46} Flexible and conformal interfaces help to reduce shear forces exhibited by repeatable micromotions due to breathing and cardiac pace at the interface.^{47,48} Polymers are the most common class of materials for neural implants, including the substrate and insulation of interconnects. This is due to their biocompatibility, flexibility, long-term stability in hostile surroundings, and little immune response to implantation.⁴⁹

Both PI and PCL have an 8 μm thickness. The mechanical properties of the polymer substrates are of utmost importance as they constitute the largest part of the device. The mechanical testing was conducted for 6 samples of both PI and PCL, where all samples had the same dimensions and thicknesses for accurate comparison (Figure 6A). The PCL and PI samples showed a Young's modulus of 24 MPa and 1.37 GPa, with a maximum tensile stress of 2.5 and 47 MPa respectively. Also, the elongation at break of the PCL substrate (4.05 mm) was higher than that of the PI substrate (0.16 mm). Both substrates exhibit flexibility and conformality, which is necessary for brain interfaces (Figure 6B,C). However, these results show that PCL is more mechanically compliant with brain tissue than several materials used for neural interfaces such as PI, Parylene C, or SU-8 (Figure 6B) and has potentially higher chances of not causing damage to tissue at the interface.

Biocompatibility. The biocompatibility of the printed devices was investigated *in vitro* using the TB assay. PC12 cells were seeded on the devices and incubated for 72 h before the TB assay was conducted. The mean number of viable cells for two independent replicates was calculated. The percentage of viable cells on the PCL, PI, and TCP positive control had similar results with 95%, 97%, and 99.5%, respectively (Figure 7A). The percentage of viable cells on PCL and PI without printed patterns were 96.2% and 98.5%, respectively. These results indicated that the PI and PCL substrates as well as the printed materials have no effect on the viability of the PC12 cells (AgNPs, PEDOT:PSS, and PVPh). The PI-based devices showed spreading cells with good adherence and numerous cell-to-cell contact similar to TCP control. In contrast, the PCL-based devices showed relatively fewer spread cells, where the majority appeared rounded. However, the spreading cells on the PCL substrates were more stretched and spindle-shaped compared to that on PI and TCP. Besides the rounded cells, it was noted that the PCL substrates also had numerous small clumps of cells. This might be due to the hydrophobic nature of the PCL surface. To induce more favorable adhesion and satisfactory cell responses, plasma treatment was used to improve the surface characteristics of the PCL substrates.^{50,51}

In addition, printed arrays (AgNPs and PEDOT:PSS) did not show cytotoxic effects on the cells, where the cells at proximity to the printed patterns were well spread (Figure 7B).

Accelerated Degradation Test. Accelerated degradation test done for PCL-based array to simulate the degradation process. Tuning the degradation rate of the interface by incorporating other biodegradable polymers can be achieved. In this work, we added PLGA to PCL to demonstrate the feasibility of the tuning process. Figure 7C shows a series of images taken at several stages of an accelerated dissolution in a buffer solution (pH 13) at 37 °C for PCL-based and PCL/PLGA-based arrays. The PCL-based array degraded within 60 h and completely disappeared after 70 h.

On the other hand, the blended PCL/PLGA array completely disappeared within less than 60 h. Therefore, this showed that blending PCL with polymers that have faster degradation rate, like PLGA, increases the overall degradation process. It is noted that the part that has the pattern on degraded last. It is important to mention that *in vitro* degradation at such high pH level is based on chemical hydrolysis only. The presence of enzymes and cells would accelerate the degradation even further.⁵² *In vivo* experiments can be conducted, in a later stage, for accurate estimation and confirmation of the degradation rate. However, on the basis of the molecular weight of the PCL used in this study, it is speculated for the array to last for about 2 years *in vivo*.²³ This is also in line with similar degradation tests carried out in the literature for neural interfaces.⁵³

Electrophysiological Recordings. The inkjet-printed devices were tested *in vitro* with isolated rat retinas for testing the potential of the device to record spiking activity. The setup is shown in Figure 8A,B. The retinas were placed on top of the device while being continually perfused with oxygenated medium before the use of white light stimuli (at 100 Hz, 100 ms). The spiking activity was recorded from GC via multiple electrodes, data shown in (Figure 8C). Spontaneous retinal activity and activity in response to light stimulation were recorded. The interspike interval (ISI) shown in Figure 8D demonstrates that the peaks of the response are found at 10 ms of the stimulus, which is typical of the retina response to stimuli.⁵⁴ Light stimuli activate the photoreceptors, which stimulate the inner retina via graded transmitter release, which in turn activates the spiking GCs. The waveform and amplitude of the spikes recorded by the devices resemble previously reported *in vitro* recording studies from the retina.^{19,20} The recorded spiking activity from GC is to our knowledge the first study that shows single-cell activity recorded from inkjet-printed devices.

CONCLUSIONS

The present study demonstrated the fabrication of a single-cell resolution, high electrochemical performance flexible neural interface array on a bioresorbable backbone. To this end, an additive, room temperature process was developed that relied on inkjet printing. The process enabled individually insulated electrodes as small as 30 μm via control over surface properties and ink formulation. Further, AgNPs/PEDOT:PSS electrodes achieved the highest electrochemical performance in the literature for any fabrication process: $\sim 200 \Omega$ impedance at 1 kHz and CSC of 2.876 C cm^{-2} for 50 μm electrodes. This is owed to the low resistance ohmic AgNPs/PEDOT:PSS interface and the additive layering of PEDOT:PSS enabled by inkjet printing while maintaining the targeted feature size.

Additional enhancement of electrode performance was also demonstrated with exfoliated graphene in PEDOT:PSS ink, which increases conductivity and surface roughness (surface area). Furthermore, the novel, additive fabrication process without harsh chemicals coupled with photonic sintering allows material selection for the interface backbone that significantly reduces the mechanical mismatch with brain tissue compared to state-of-the-art polymer-based interfaces. For our interface, we used bioresorbable PCL, a reduction in Young's modulus of 3 orders of magnitude compared to commonly used polyimide or parylene. Not only does mechanical mismatch between the tissue and interface cause damage due to stresses on the target tissue, but also limited conformability to curved brain tissue (like for surface recordings) can increase the distance to the target cell and reduce recording and stimulation resolution. Also, the selection of a bioresorbable backbone lessens tissue damage from possible implant resection. Finally, we showed that the final devices are biocompatible *in vitro* and capable of recording a single cell from an isolated rat retina preparation.

In conclusion, the room temperature fabrication process without harsh chemicals enables the selection of a wide range of materials for interface backbone and electrodes that can have a significant impact on interface life and performance. This will help in addressing several challenges facing neural implants. Also, the potential for building a high performance, high spatial, and single-cell resolution neural interface with the novel, low cost, and easily customizable additive manufacturing can change the way we build these devices for either electrophysiological monitoring or clinical applications. The next step is testing the inkjet-printed device in animal models along with testing long-term stability and durability.

■ ASSOCIATED CONTENT

SI Supporting Information

The Supporting Information is available free of charge at <https://pubs.acs.org/doi/10.1021/acsabm.0c00895>.

Printing parameters, biocompatibility, and electrochemical tests (PDF)

■ AUTHOR INFORMATION

Corresponding Author

Massoud L. Khraiche – *Neural Engineering and Nanobiosensors Group, Biomedical Engineering Program, Maroun Semaan Faculty of Engineering and Architecture, American University of Beirut, Beirut 1107 2020, Lebanon;* orcid.org/0000-0002-4497-3168; Email: mkhraiche@aub.edu.lb

Authors

Reem M. Almasri – *Neural Engineering and Nanobiosensors Group, Biomedical Engineering Program, Maroun Semaan Faculty of Engineering and Architecture, American University of Beirut, Beirut 1107 2020, Lebanon;* orcid.org/0000-0003-3530-8323

Walid AlChamaa – *Neural Engineering and Nanobiosensors Group, Biomedical Engineering Program, Maroun Semaan Faculty of Engineering and Architecture, American University of Beirut, Beirut 1107 2020, Lebanon;* orcid.org/0000-0001-6997-4469

Ali Reza Tehrani-Bagha – *Department of Chemical Engineering and Advanced Energy, American University of*

Beirut, Beirut 1107 2020, Lebanon; orcid.org/0000-0002-8206-3827

Complete contact information is available at: <https://pubs.acs.org/10.1021/acsabm.0c00895>

Author Contributions

R.A., Conceptualization, Methodology, Investigation, Writing - Original Draft, Visualization, Formal analysis. W.A., small part Methodology. Small part Investigation. Small part Formal analysis. A.T., small part Methodology. Small part Resources. M.K., Conceptualization, Writing - Original Draft - Review & Editing, Funding acquisition, Project administration, Supervision, Resources, Visualization, Investigation, Methodology.

Notes

The authors declare no competing financial interest.

■ ACKNOWLEDGMENTS

The authors thank the staff at Central Research Science Laboratory (CRSL) at American University of Beirut for their continuous support. The authors gratefully acknowledge the assistance and support from Daniel Maher and Zeina Habli in some of the characterization and biocompatibility experiments.

■ ABBREVIATIONS

AgNPs, silver nanoparticles
CSC, charge storage capacity
PCL, polycaprolactone
PI, polyimide
PEDOT:PSS, (3,4-ethylenedioxythiophene)-poly(styrenesulfonate)

■ REFERENCES

- (1) Stacey, W. C.; Litt, B. Technology insight: neuroengineering and epilepsy—designing devices for seizure control. *Nat. Clin. Pract. Neurol.* **2008**, *4* (4), 190–201.
- (2) Oxley, T. J.; Opie, N. L.; John, S. E.; Rind, G. S.; Ronayne, S. M.; Wheeler, T. L.; Judy, J. W.; McDonald, A. J.; Dornom, A.; Lovell, T. J.; et al. Minimally invasive endovascular stent-electrode array for high-fidelity, chronic recordings of cortical neural activity. *Nat. Biotechnol.* **2016**, *34* (3), 320–327.
- (3) Yu, K. J.; Kuzum, D.; Hwang, S.-W.; Kim, B. H.; Juul, H.; Kim, N. H.; Won, S. M.; Chiang, K.; Trumpis, M.; Richardson, A. G.; et al. Bioresorbable silicon electronics for transient spatiotemporal mapping of electrical activity from the cerebral cortex. *Nat. Mater.* **2016**, *15* (7), 782.
- (4) Alt, M. T.; Fiedler, E.; Rudmann, L.; Ordonez, J. S.; Ruther, P.; Stieglitz, T. Let there be light—optoprobes for neural implants. *Proc. IEEE* **2017**, *105* (1), 101–138.
- (5) DUPONT. *Kapton 30HN Datasheet*; 2011.
- (6) Khraiche, M. L.; Phillips, W. B.; Jackson, N.; Muthuswamy, J. Sustained elevation of activity of developing neurons grown on polyimide microelectrode arrays (MEA) in response to ultrasound exposure. *Microsyst. Technol.* **2017**, *23* (8), 3671–3683.
- (7) Bilston, L. E. *Neural tissue biomechanics*; Springer Science & Business Media: 2011; Vol. 3.
- (8) Cummins, G.; Desmulliez, M. P. Y. Inkjet printing of conductive materials: a review. *Circuit World* **2012**, *38* (4), 193–213.
- (9) Garma, L. D.; Ferrari, L. M.; Scognamiglio, P.; Greco, F.; Santoro, F. Inkjet-printed PEDOT:PSS multi-electrode arrays for low-cost *in vitro* electrophysiology. *Lab Chip* **2019**, *19* (22), 3776–3786.
- (10) Adly, N.; Weidlich, S.; Seyock, S.; Brings, F.; Yakushenko, A.; Offenhäusser, A.; Wolfrum, B. Printed microelectrode arrays on soft materials: from PDMS to hydrogels. *npj Flexible Electronics* **2018**, *2* (1), 1–9.

- (11) Bachmann, B.; Adly, N. Y.; Schnitker, J.; Yakushenko, A.; Rinklin, P.; Offenhäusser, A.; Wolfrum, B. All-inkjet-printed gold microelectrode arrays for extracellular recording of action potentials. *Flexible and Printed Electronics* **2017**, *2* (3), 035003.
- (12) Kokubo, N.; Arake, M.; Yamagishi, K.; Morimoto, Y.; Takeoka, S.; Ohta, H.; Fujie, T. Inkjet-printed neural electrodes with mechanically gradient structure. *ACS Applied Bio Materials* **2019**, *2* (1), 20–26.
- (13) Cellot, G.; Lagonegro, P.; Tarabella, G.; Scaini, D.; Fabbri, F.; Iannotta, S.; Prato, M.; Salviati, G.; Ballerini, L. PEDOT: PSS interfaces support the development of neuronal synaptic networks with reduced neuroglia response in vitro. *Front. Neurosci.* **2016**, *9*, 521.
- (14) Cui, X. T.; Zhou, D. D. Poly (3, 4-ethylenedioxythiophene) for chronic neural stimulation. *IEEE Transactions on Neural Systems and Rehabilitation Engineering* **2007**, *15* (4), 502–508.
- (15) Vosgueritchian, M.; Lipomi, D. J.; Bao, Z. Highly conductive and transparent PEDOT: PSS films with a fluorosurfactant for stretchable and flexible transparent electrodes. *Adv. Funct. Mater.* **2012**, *22* (2), 421–428.
- (16) Ludwig, K. A.; Uram, J. D.; Yang, J.; Martin, D. C.; Kipke, D. R. Chronic neural recordings using silicon microelectrode arrays electrochemically deposited with a poly (3, 4-ethylenedioxythiophene)(PEDOT) film. *Journal of neural engineering* **2006**, *3* (1), 59.
- (17) Kim, J.; Jung, J.; Lee, D.; Joo, J. Enhancement of electrical conductivity of poly (3, 4-ethylenedioxythiophene)/poly (4-styrenesulfonate) by a change of solvents. *Synth. Met.* **2002**, *126* (2–3), 311–316.
- (18) Tevi, T.; Saint Birch, S. W.; Thomas, S. W.; Takshi, A. Effect of Triton X-100 on the double layer capacitance and conductivity of poly (3, 4-ethylenedioxythiophene): poly (styrenesulfonate)(PEDOT: PSS) films. *Synth. Met.* **2014**, *191*, 59–65.
- (19) Ha, S.; Khraiche, M. L.; Akinin, A.; Jing, Y.; Damle, S.; Kuang, Y.; Bauchner, S.; Lo, Y. H.; Freeman, W. R.; Silva, G. A.; Cauwenberghs, G. Towards high-resolution retinal prostheses with direct optical addressing and inductive telemetry. *J. Neural Eng.* **2016**, *13* (5), 056008.
- (20) Ha, S.; Khraiche, M. L.; Silva, G. A.; Cauwenberghs, G. Direct inductive stimulation for energy-efficient wireless neural interfaces. *Conf Proc. IEEE Eng. Med. Biol. Soc.* **2012**, *2012*, 883–886.
- (21) Quiroga, R. Q.; Nadasdy, Z.; Ben-Shaul, Y. Unsupervised spike detection and sorting with wavelets and superparamagnetic clustering. *Neural computation* **2004**, *16* (8), 1661–1687.
- (22) Khraiche, M.; Muthuswamy, J. Multi-modal biochip for simultaneous, real-time measurement of adhesion and electrical activity of neurons in culture. *Lab Chip* **2012**, *12* (16), 2930–41.
- (23) Pitt, C.; Chasalow, F.; Hibionada, Y.; Klimas, D.; Schindler, A. Aliphatic polyesters. I. The degradation of poly (ϵ -caprolactone) in vivo. *J. Appl. Polym. Sci.* **1981**, *26* (11), 3779–3787.
- (24) Hernández, A. R.; Contreras, O. C.; Acevedo, J. C.; Moreno, L. G. N. Poly (ϵ -caprolactone) degradation under acidic and alkaline conditions. *Am. J. Polym. Sci.* **2013**, *3* (4), 70.
- (25) Ganji, M.; Kaestner, E.; Hermiz, J.; Rogers, N.; Tanaka, A.; Cleary, D.; Lee, S. H.; Snider, J.; Halgren, M.; Cosgrove, G. R.; et al. Development and translation of PEDOT: PSS microelectrodes for intraoperative monitoring. *Adv. Funct. Mater.* **2018**, *28* (12), 1700232.
- (26) Yang, W.; Broski, A.; Wu, J.; Fan, Q. H.; Li, W. Characteristics of transparent, PEDOT: PSS-coated indium-tin-oxide (ITO) microelectrodes. *IEEE Trans. Nanotechnol.* **2018**, *17* (4), 701–704.
- (27) Koutsouras, D. A.; Gkoupidenis, P.; Stolz, C.; Subramanian, V.; Malliaras, G. G.; Martin, D. C. Impedance Spectroscopy of Spin-Cast and Electrochemically Deposited PEDOT: PSS Films on Micro-fabricated Electrodes with Various Areas. *ChemElectroChem* **2017**, *4* (9), 2321–2327.
- (28) Castagnola, E.; Marrani, M.; Maggiolini, E.; Maita, F.; Pazzini, L.; Polese, D.; Pecora, A.; Maiolo, L.; Fortunato, G.; Fadiga, L.; et al. Recording high frequency neural signals using conformable and low-impedance ECoG electrodes arrays coated with PEDOT-PSS-PEG. *Adv. Sci. Technol.* **2016**, *102*, 77–85.
- (29) Wang, J.; Fei, F.; Luo, Q.; Nie, S.; Wu, N.; Chen, X.; Su, W.; Li, Y.; Ma, C. Q. Modification of the Highly Conductive PEDOT:PSS Layer for Use in Silver Nanogrid Electrodes for Flexible Inverted Polymer Solar Cells. *ACS Appl. Mater. Interfaces* **2017**, *9* (8), 7834–7842.
- (30) Tian, H.-C.; Liu, J.-Q.; Wei, D.-X.; Kang, X.-Y.; Zhang, C.; Du, J.-C.; Yang, B.; Chen, X.; Zhu, H.-Y.; NuLi, Y.-N.; et al. Graphene oxide doped conducting polymer nanocomposite film for electrode-tissue interface. *Biomaterials* **2014**, *35* (7), 2120–2129.
- (31) Bhandari, S.; Deepa, M.; Srivastava, A. K.; Lal, C.; Kant, R. Poly (3, 4-ethylenedioxythiophene)(PEDOT)-Coated MWCNTs Tethered to Conducting Substrates: Facile Electrochemistry and Enhanced Coloring Efficiency. *Macromol. Rapid Commun.* **2008**, *29* (24), 1959–1964.
- (32) Luo, X.; Weaver, C. L.; Tan, S.; Cui, X. T. Pure graphene oxide doped conducting polymer nanocomposite for bio-interfacing. *J. Mater. Chem. B* **2013**, *1* (9), 1340–1348.
- (33) Khraiche, M. L.; Jackson, N.; Muthuswamy, J. Early onset of electrical activity in developing neurons cultured on carbon nanotube immobilized microelectrodes. *Conf Proc. IEEE Eng. Med. Biol. Soc.* **2009**, *2009*, 777–80.
- (34) Khraiche, M. L.; Rogul, J.; Muthuswamy, J. Design and Development of Microscale Thickness Shear Mode (TSM) Resonators for Sensing Neuronal Adhesion. *Front. Neurosci.* **2019**, *13*, 518.
- (35) Shi, L.; Layani, M.; Cai, X.; Zhao, H.; Magdassi, S.; Lan, M. An inkjet printed Ag electrode fabricated on plastic substrate with a chemical sintering approach for the electrochemical sensing of hydrogen peroxide. *Sens. Actuators, B* **2018**, *256*, 938–945.
- (36) Bergman, T. L.; Incropera, F. P. *Fundamentals of heat and mass transfer*, 7th ed.; Wiley: Hoboken, NJ, 2011; p xxiii, 1048 p.
- (37) Bejan, A. *Convection heat transfer*; John Wiley & Sons, 2013.
- (38) Rager, M. S.; Aytug, T.; Veith, G. M.; Joshi, P. Low-Thermal-Budget Photonic Processing of Highly Conductive Cu Interconnects Based on CuO Nanoinks: Potential for Flexible Printed Electronics. *ACS Appl. Mater. Interfaces* **2016**, *8* (3), 2441–8.
- (39) Agari, Y.; Ueda, A. Thermal conductivity of poly (vinyl chloride)/polycaprolactone blends. *J. Polym. Sci., Part B: Polym. Phys.* **1994**, *32* (1), 59–62.
- (40) Hetke, J. F.; Lund, J. L.; Najafi, K.; Wise, K. D.; Anderson, D. J. Silicon ribbon cables for chronically implantable microelectrode arrays. *IEEE Trans. Biomed. Eng.* **1994**, *41* (4), 314–321.
- (41) Najafi, K.; Ji, J.; Wise, K. Scaling limitations of silicon multichannel recording probes. *IEEE Trans. Biomed. Eng.* **1990**, *37* (1), 1–11.
- (42) Robinson, D. A. The electrical properties of metal microelectrodes. *Proc. IEEE* **1968**, *56* (6), 1065–1071.
- (43) Szarowski, D.; Andersen, M.; Retterer, S.; Spence, A.; Isaacson, M.; Craighead, H.; Turner, J.; Shain, W. Brain responses to micro-machined silicon devices. *Brain Res.* **2003**, *983* (1–2), 23–35.
- (44) Turner, C. H.; Rho, J.; Takano, Y.; Tsui, T. Y.; Pharr, G. M. The elastic properties of trabecular and cortical bone tissues are similar: results from two microscopic measurement techniques. *J. Biomech.* **1999**, *32* (4), 437–441.
- (45) Lee, H.; Bellamkonda, R. V.; Sun, W.; Levenston, M. E. Biomechanical analysis of silicon microelectrode-induced strain in the brain. *Journal of neural engineering* **2005**, *2* (4), 81.
- (46) Hoogerwerf, A. C.; Wise, K. D. A three-dimensional microelectrode array for chronic neural recording. *IEEE Trans. Biomed. Eng.* **1994**, *41* (12), 1136–1146.
- (47) Yeager, J. D.; Phillips, D. J.; Rector, D. M.; Bahr, D. F. Characterization of flexible ECoG electrode arrays for chronic recording in awake rats. *J. Neurosci. Methods* **2008**, *173* (2), 279–285.
- (48) Lee, J. H.; Kim, H.; Kim, J. H.; Lee, S. H. Soft implantable microelectrodes for future medicine: prosthetics, neural signal recording and neuromodulation. *Lab Chip* **2016**, *16* (6), 959–76.
- (49) Hassler, C.; Boretius, T.; Stieglitz, T. Polymers for neural implants. *J. Polym. Sci., Part B: Polym. Phys.* **2011**, *49* (1), 18–33.

(50) Siri, S.; Wadbua, P.; Amornkitbamrung, V.; Kampa, N.; Maensiri, S. Surface modification of electrospun PCL scaffolds by plasma treatment and addition of adhesive protein to promote fibroblast cell adhesion. *Mater. Sci. Technol.* **2010**, *26* (11), 1292–1297.

(51) Yan, D.; Jones, J.; Yuan, X.; Xu, X.; Sheng, J.; Lee, J. M.; Ma, G.; Yu, Q. Plasma treatment of electrospun PCL random nanofiber meshes (NFMs) for biological property improvement. *J. Biomed. Mater. Res., Part A* **2013**, *101* (4), 963–972.

(52) Mochizuki, M.; Hirano, M.; Kanmuri, Y.; Kudo, K.; Tokiwa, Y. Hydrolysis of polycaprolactone fibers by lipase: effects of draw ratio on enzymatic degradation. *J. Appl. Polym. Sci.* **1995**, *55* (2), 289–296.

(53) Yu, K. J.; Kuzum, D.; Hwang, S. W.; Kim, B. H.; Juul, H.; Kim, N. H.; Won, S. M.; Chiang, K.; Trumpis, M.; Richardson, A. G.; Cheng, H.; Fang, H.; Thomson, M.; Bink, H.; Talos, D.; Seo, K. J.; Lee, H. N.; Kang, S. K.; Kim, J. H.; Lee, J. Y.; Huang, Y.; Jensen, F. E.; Dichter, M. A.; Lucas, T. H.; Viventi, J.; Litt, B.; Rogers, J. A. Bioresorbable silicon electronics for transient spatiotemporal mapping of electrical activity from the cerebral cortex. *Nat. Mater.* **2016**, *15* (7), 782–791.

(54) Berry, M. J.; Warland, D. K.; Meister, M. The structure and precision of retinal spike trains. *Proc. Natl. Acad. Sci. U. S. A.* **1997**, *94* (10), 5411–5416.